Optical and Field-Emission Properties of ZnO Nanostructures Deposited Using High-Pressure Pulsed Laser Deposition

T. Premkumar,*,[†] Y. S. Zhou,[‡] Y. F. Lu,[‡] and K. Baskar[†]

Crystal Growth Centre, Anna University, Chennai, 600 025, Tamilnadu, India, and Department of Electrical Engineering, University of Nebraska−Lincoln, Lincoln, Nebraska 68588-0511

ABSTRACT ZnO nanostructures were deposited on GaN (0001), Al_2O_3 (0001), and Si (100) substrates using a high-pressure pulsed laser deposition (PLD) method. Vertically aligned hexagonal−pyramidal ZnO nanorods were obtained on the Al_2O_3 and Si substrates whereas interlinked ZnO nanowalls were obtained on the GaN substrates. A growth mechanism has been proposed for the formation of ZnO nanowalls based on different growth rates of ZnO polar and nonpolar planes. Both ZnO nanorods and nanowalls exhibit a strong E_{2H} vibration mode in the micro-Raman spectra. The corresponding fluorescence spectra of ZnO nanorods and nanowalls showed near band emission at 3.28 eV. The ZnO nanorods grown on the Si substrates exhibited better crystalline and optical properties compared with the ZnO structures grown on the GaN and Al_2O_3 substrates. The high aspect ratio, good vertical alignment, and better crystallinity of the ZnO nanorods with tapered tips exhibited promising field emission performance with a low turn-on field of 2 V/μm, a high current density of 7.7 mA/cm^2, and a large field enhancement factor.

KEYWORDS: zinc oxide • high-pressure pulsed laser deposition • nanowalls • nanorod field-emission properties • optical properties

1. INTRODUCTION

One-dimensional (1D) semiconductor nanostructures have attracted much interest because of their remarkable physical and chemical properties in the nanoscale regime. Among them, ZnO nanostructures, which have a bandgap of 3.37 eV and an exciton binding energy of 60 meV, have potential applications in nanoelectronics (1), nano-optelectronics (2), nanopiezotronics (3), gas/chemical sensors (4), transparent electrodes (5), and field emission devices (6). Various forms of ZnO nanostructures, including nanorods (7, 8), nanowalls (9), nanowires (10), nanobelts (11), and quantum dots (12), have been reported using physical and chemical deposition techniques. In comparison with ZnO nanorods/wires, the growth of two-dimensional (2D) ZnO nanowalls are difficult due to its polar structure along the c-axis. The basal plane of (0001) has the highest surface energy that induces the fast growth along the c-axis direction which results in the 1D nanorod/wire growth. From the practical point of view, ZnO nanowalls are interesting because of their large surface area and potential applications in gas/chemical sensors and field emission devices. Until now, only a few papers have reported the growth of ZnO nanowall arrays. Ng et al. (13) claimed the reproducible growth of ZnO nanowalls and nanorods using a carbothermal reduction process and gold-catalyzed epitaxial growth. Hong et al. (9) demonstrated the reproducible growth of ZnO nanowalls and nanotubes using a conventional lithography and catalyst free metal organic vapor phase epitaxy (MOVPE) technique. Kim et al. (14) confirmed the formation of ZnO thin film prior to the growth of ZnO nanowalls on GaN substrates. It was also reported that the nucleation at the tip of the grain surface (15) and phosphorus doping in ZnO (16) would induce the growth of ZnO nanowalls. The origin of the growth of ZnO nanowalls is still under debate.

In this study, we carried out the synthesis of ZnO nanowalls and nanorods using high-pressure pulsed laser deposition (PLD). The surface morphology and structural and optical properties of the ZnO nanowalls and nanorods were investigated using field emission scanning electron microscopy (FE-SEM), X-ray diffraction (XRD), and micro-Raman and fluorescence spectroscopy. The ZnO nanorods show good field emission characteristics with high field enhancement factor (β) compared with ZnO nanowalls. The mechanisms for the formation of ZnO nanowalls were also discussed on the basis of the different growth rates of ZnO polar and nonpolar planes.

2. EXPERIMENTAL SECTION

ZnO nanostructures were grown on GaN (0001), Al_2O_3 (0001), and Si (100) substrates, respectively, using a commercial PLD system (Neocera, Pioneer 180). The substrates were cleaned using acetone and methanol sequentially for 3 min, rinsed with distilled water (DI), and dried in an atmosphere before being loaded into the chamber. The chamber was evacuated to a base pressure of 8 × 10^{-6} Torr after loading the ZnO target and substrates. A KrF excimer laser (Lambda Physik Compex 205; λ = 248 nm; fluence, -3 J/cm^2; pulse duration, -30 ns; re-
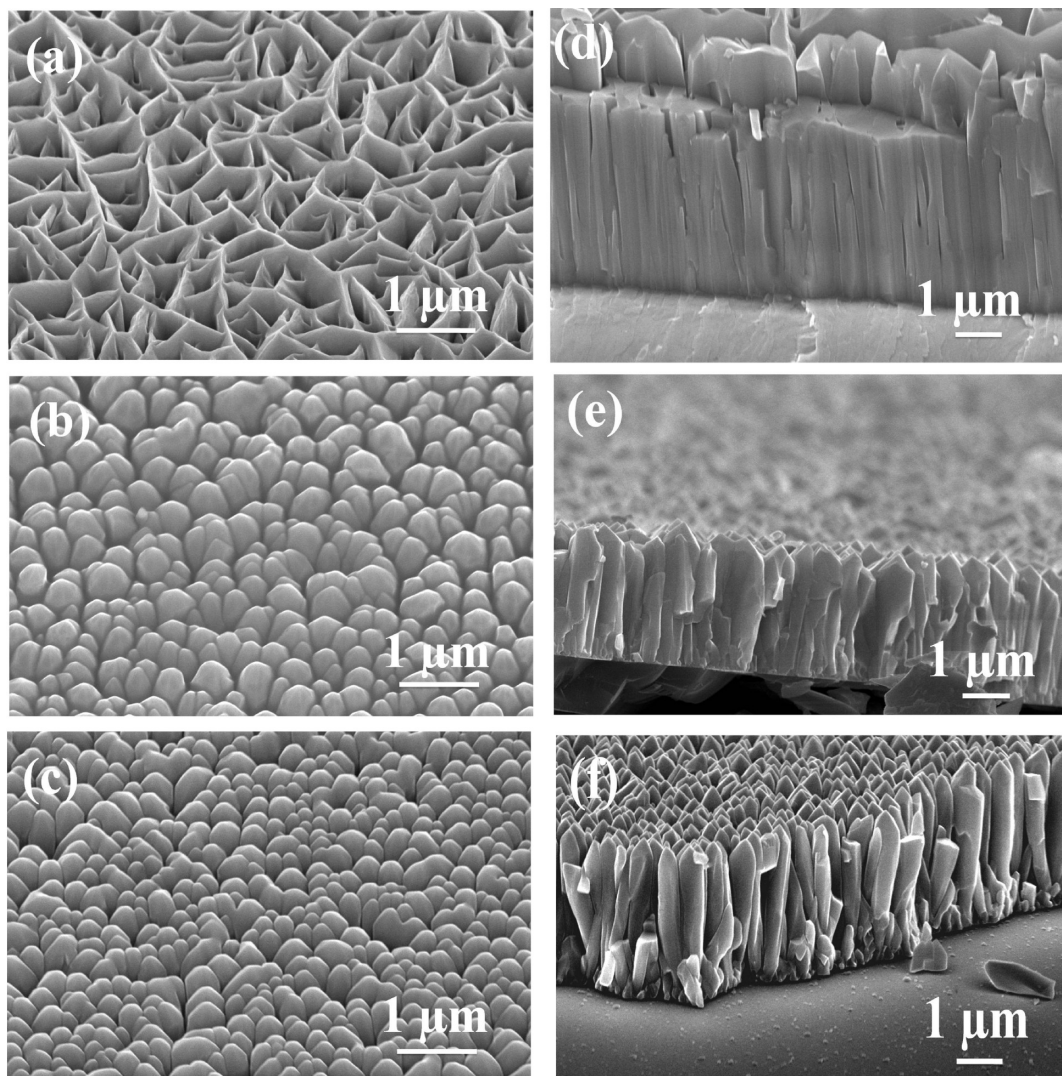
2010 American Chemical Society

FIGURE 1. FE-SEM images of ZnO nanowalls and nanorods: (a−c) 45° tilted and (d−f) cross-sectional views of ZnO nanostructures grown on GaN, Al_2O_3, and Si.

petition rate, -10 Hz) was used as an excitation source to irradiate the ZnO target. The laser beam was focused onto the ZnO target through a quartz window at an incidence angle of 45°. The substrates were placed at 25 mm away from the target. The chamber was maintained at an oxygen pressure of 7 Torr during the deposition. The ZnO films were deposited with two different durations of 30 and 20 min. The as-grown samples were subjected to different characterizations as follows. The field-emission scanning electron microscopy (FE-SEM, Hitachi S4700 system, with a resolution of 1.2 nm at 25 kV) was performed to observe the morphology and dimensions of the ZnO nanostructures. The crystalline property and structure of the nanostructures were studied using a micro-Raman spectrometer (Renishaw Invia; spatial resolution, $-1 \ \mu m$) with an argon ion laser ($\lambda = 514.5$ nm) as an excitation source and an X-ray diffractometer (Rigaku D/Max B diffractometer, Cu Kα, $\lambda = 1.54$ Å). The optical properties of the ZnO nanowalls and nanorods were studied using a fluorimeter (Shimadzu-RF 5301PC, xenon source, the excitation wavelength is $\lambda = 325$ nm). The field-emission (FE) characteristics of the ZnO nanowalls and nanorods deposited on the GaN and Si substrates were measured in a two-parallel-plate configuration. Initially, the vacuum chamber was evacuated to a base pressure of 1.5×10^{-5} Torr, and then, the chamber was purged with argon gas to remove any residual gases. The voltage was swept manually between the electrodes using a Keithley 2410c source meter from 0 to 500 V to test any short circuit between the electrodes. After this test, the voltage was swept using the automatic sweep option in the source meter from 0 to 1000 V. This experiment was repeated several times to check the consistency of the results.

3. RESULTS AND DISCUSSION

3.1. Morphology and Growth Mechanism of ZnO Nanowalls and Nanorods.
Figure 1a−f shows the SEM micrographs of the ZnO nanowalls and nanorods grown on the GaN, Al_2O_3, and Si substrates, respectively, at a growth period of 30 min. Figure 1a−c shows the 45° tilted view, and Figure 1d−f shows the cross-sectional view of the ZnO nanowalls and nanorods. The vertically aligned ZnO nanorods were obtained on the Al_2O_3 and Si substrates. The diameter and length of the ZnO nanorods were 300 ± 50 nm and $3 \pm 0.1 \ \mu m$, respectively. The interlinked ZnO nanowalls were obtained on the GaN substrate. The width and height of the ZnO nanowalls were 120 ± 50 nm and $1.2 \pm 0.1 \ \mu m$, respectively.

Several parameters would influence the nucleation of the ZnO nanostructures, including the lattice mismatch between the substrate and the film, the substrate temperature, and the oxygen partial pressure. During the growth, at a fixed substrate temperature and oxygen pressure, the key parameter affecting the nucleation process is the lattice mismatch between the film and the substrate. Verma et al. (17) reported a well separated ZnO nanocolumn on Al_2O_3 substrate (lattice mismatch, -26%) and columnar thin films on yttrium stabilized zircoina substrate (lattice mismatch, -8%). The diameter increase and coalescence of the nanocolumns were attributed to the decrease in the lattice mismatch between the film and substrate (17). The lattice mismatch between ZnO and GaN, Al_2O_3 and Si are 1.8%, 18.4%, and 40.1%, respectively (18). In this study, ZnO morphology transformed from nanorods to nanowalls with a decrease in the lattice mismatch between the substrates and films. The lattice mismatch effect between ZnO and Si was not considered to be genuine because of the formation of native oxide layer on Si. These results correlate well with the work by Verma et al. (17). The cross-sectional view in Figure 1d shows the growth of dense ZnO columnar film on GaN compared with Al_2O_3 and Si substrates. No individual ZnO nanorods were observed on GaN. This behavior can be attributed to the low lattice mismatch between ZnO and GaN. Okada et al. have also shown the change in morphology and orientation of ZnO nanostructures with respect to substrates (7). This implies that the morphologies of ZnO nanostructures can be tuned during growth by utilizing the lattice mismatch between the substrate and film.

Figure 2 shows a schematic diagram for the growth mechanism of the ZnO nanowalls. Laser ablation of the ZnO target in high oxygen pressure of ~7 Torr led to the formation of nanoparticles in the gas phase due to a large number of collisions among ablated species and gas molecules. These nanoparticles acted as nucleation sites during the growth of nanorods (Figure 2a,b) (19). Due to the polar nature of ZnO, the nanorods grew preferentially along [0001] directions because of the high surface energy of (0001) facets. The growth rates of ZnO crystals in different directions have been reported showing the following tendency, $[0001] > [01\bar{1}\bar{1}] > [10\bar{1}0] > [01\bar{1}1]$ under hydrothermal conditions (20, 21), resulting in crystals being bounded by $(10\bar{1}0)$ facets with $[01\bar{1}1]$ caps. The growth rate along $\langle 0001 \rangle$ directions is higher than that of $<10\bar{1}0 >$ and $<01\bar{1}1 >$ directions. Similarly, $(10\bar{1}0)$ and (0001) facets are generally observed in ZnO nanostructures; this correlates well with the present results. While nanorods grow along the vertical direction, the incoming ablated Zn and O species contributed to the radial growth of nanorods along the $<10\bar{1}0 >$ direction. The radial growth leads to coalescing of neighboring nanorods with each other; after coalescence, there is no growth along $<10\bar{1}0 >$ direction. The growth is presumed to continue along the $<01\bar{1}1 >$ direction, as shown in Figure 2c and d. Laudise et al. (22) reported that the growth rate for the $<01\bar{1}1 >$ direction seemed to be intermediate between those of $<10\bar{1}0 >$ and $\langle 0001 \rangle$ directions. Further growth along the
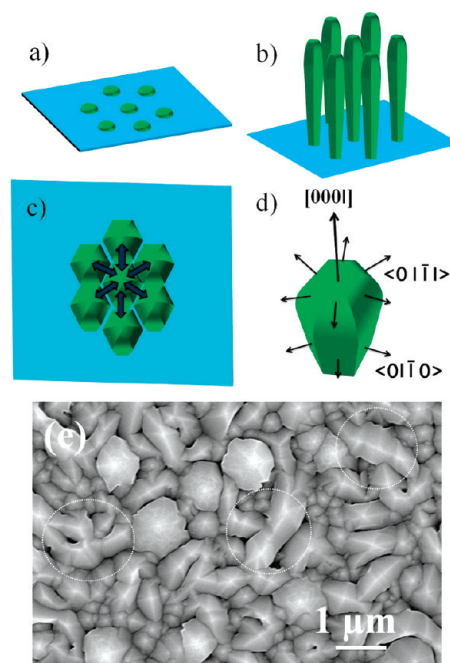

FIGURE 2. Schematic representation of growth mechanism of ZnO nanowalls. (a) ZnO nanoparticles deposited on the substrate. (b) Growth of ZnO nanorods/columnar thin films. (c) Left-right arrow represents the formation of nanobridges/walls. (d) Planes of the Wurtzite ZnO. (e) FE-SEM images of ZnO grown on GaN substrate for 20 min.

$<01\bar{1}1 >$ direction among the tips of the nanorods leads to formation of bridges (15). Finally, the interlinked network of nanowalls was formed over the dense columnar ZnO films. The formation of ZnO thin films prior to the growth of nanowalls was reported by several groups (14). Similarly, in this study, dense columnar ZnO films were observed on GaN substrates before the formation of nanowalls.

ZnO was deposited for 20 min with the other growth parameters kept the same to confirm the formation of bridges between the tips of ZnO nanorods. Figure 2e shows the top view of the ZnO nanowalls grown on the GaN substrates. The circle represents an initial stage of the formation of ZnO nanowalls/bridges. Figure 2e clearly shows the top of ZnO nanorods and bridges connecting the nanorod tips. The lateral growth of nanorods along the $<01\bar{1}1 >$ direction connects all of them together and evolves as nanowalls along the c-axis.

3.2. Structural and Optical Properties. Figure 3 shows the X-ray diffraction pattern of the ZnO nanowalls and nanorods grown on the GaN, Al_2O_3, and Si substrates. In addition to substrate peaks, ZnO nanostructures show strong peaks corresponding to ZnO (0002) and (0004) planes. The strong (0002) peak shows that the ZnO nanostructures were preferentially oriented along the c-axis. Since the lattice constants of ZnO and GaN are very close to each other, overlapping can be observed for (0002) peaks of GaN and ZnO (23). The preferred orientation of ZnO nanostructures along (0002) indicates that the as grown nanostructures have good epitaxial orientation with the GaN, Al_2O_3, and Si substrates.
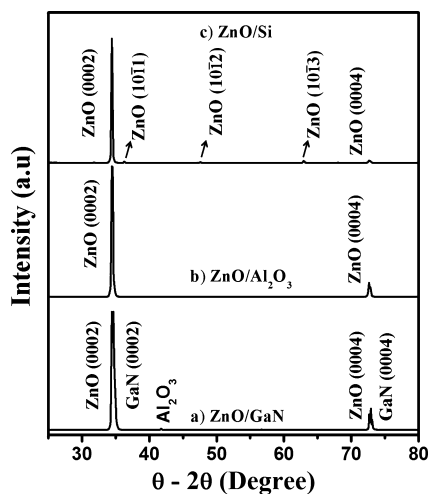
FIGURE 3. X-ray diffraction pattern of ZnO nanostructures grown on (a) GaN, (b) Al_2O_3, and (c) Si substrates.
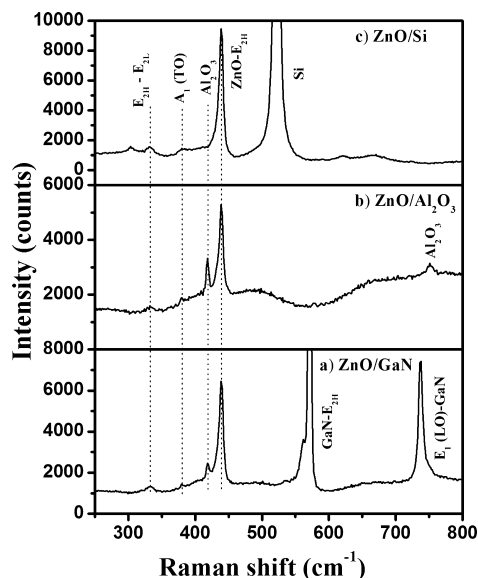

FIGURE 4. Micro-Raman spectra of ZnO nanostructures grown on (a) GaN, (b) Al_2O_3, and (c) Si substrates.

Wurtzite ZnO belongs to space group C_{6v} with two formula units per primitive cell. Group theory shows that the Raman active modes are $A_1 + E_1 + 2E_2$, where two nonpolar E_2 modes are Raman active, and A_1 and E_1 modes are both Raman and infrared active. The high-frequency E_{2H} mode involves the vibration of oxygen (O) atoms, while low-frequency E_{2L} mode is associated with the vibration of the zinc (Zn) sublattice (24). The vibrational modes of the as grown ZnO nanostructures were observed using micro-Raman spectroscopy. Figure 4 shows the micro-Raman spectra of ZnO nanostructures grown on the GaN, Al_2O_3, and Si substrates. Raman shifts of ZnO were observed at 331 ($E_{2H} - E_{2L}$), 380 (A_1 (TO)), and 439 cm^{-1} (E_{2H}) (25). The Raman shifts observed at 417, 521, 571, and 736 cm^{-1} correspond to Al_2O_3, Si, GaN (E_{2H}), and GaN (A_1 (LO)), respectively. The E_{2H} mode of ZnO nanowalls and nanorods were observed at 439 cm^{-1}. The strong E_{2H} mode can be attributed to low intrinsic defects associated with O, e.g., O vacancies (V_O), since E_{2H} mode is only associated with the vibration of O
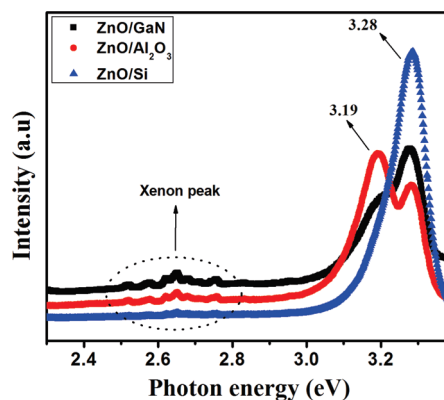

FIGURE 5. Fluorescence spectra of ZnO nanostructures grown on GaN, Al_2O_3, and Si substrates.

atoms (25). The low V_O in the ZnO nanorods and nanowalls can be attributed to the high oxygen pressure during PLD growth. The intensity of E_{2H} mode of ZnO nanorods grown on Si is higher than that of ZnO grown on the GaN and Al_2O_3 substrates. This indicates that the ZnO nanorods grown on Si have better crystallinity compared with the nanowalls and nanorods grown on the GaN and Al_2O_3 substrates.

Figure 5 compares the fluorescence spectra of the ZnO nanowalls and nanorods grown on the GaN, Al_2O_3, and Si substrates. The spectra show a strong near-band-edge (NBE) emission of ZnO at 3.28 eV which is closer to the bandgap of bulk ZnO (3.36 eV). A set of sharp peaks found between 2.5 and 2.8 eV arise due to the xenon lamp spectrum (26). In addition to the NBE emission, a peak at 3.19 eV is observed for ZnO grown on GaN and Al_2O_3. Similarly, Lin et al. (27) reported the energy level of zinc vacancy (V_{Zn}) at 3.06 eV below the conduction band. In this study, the peak located at 3.19 eV closely matched with V_{Zn}. The formation of oxygen vacancy (V_O) and zinc interstitials (Zn_i) are high in ZnO grown under low oxygen pressures. The formation of zinc vacancy (V_{Zn}), oxygen interstitials (O_i), and oxygen antisite (O_{Zn}) are high in ZnO grown under high oxygen pressures (28). Though formation of O_i and O_{Zn} are also favorable in the present case, the energy intervals between these defect levels and the conduction band edge are 2.28 and 2.38 eV, respectively. Hence, these energy levels are too small to assign to the violet emission. Therefore, emission peak at 3.19 eV observed in this study can be assigned to electron transition from the bottom of the conduction band to the Zn vacancy level (27). No deep level emissions such as V_O and Zn_i were observed for the ZnO nanorods and nanowalls in the visible region. The presence of V_{Zn} and absence of V_O and Zn_i levels in ZnO nanowalls and nanorods can be due to high oxygen pressure during the growth of ZnO nanostructures. These results are in good agreement with the micro-Raman data. The ZnO nanorods grown on Si have strong NBE emission, strong E_{2H} mode, and low V_{Zn} compared with those on GaN and Al_2O_3. Further investigations are required to understand the reason behind the better crystalline and optical properties of ZnO nanorods grown on
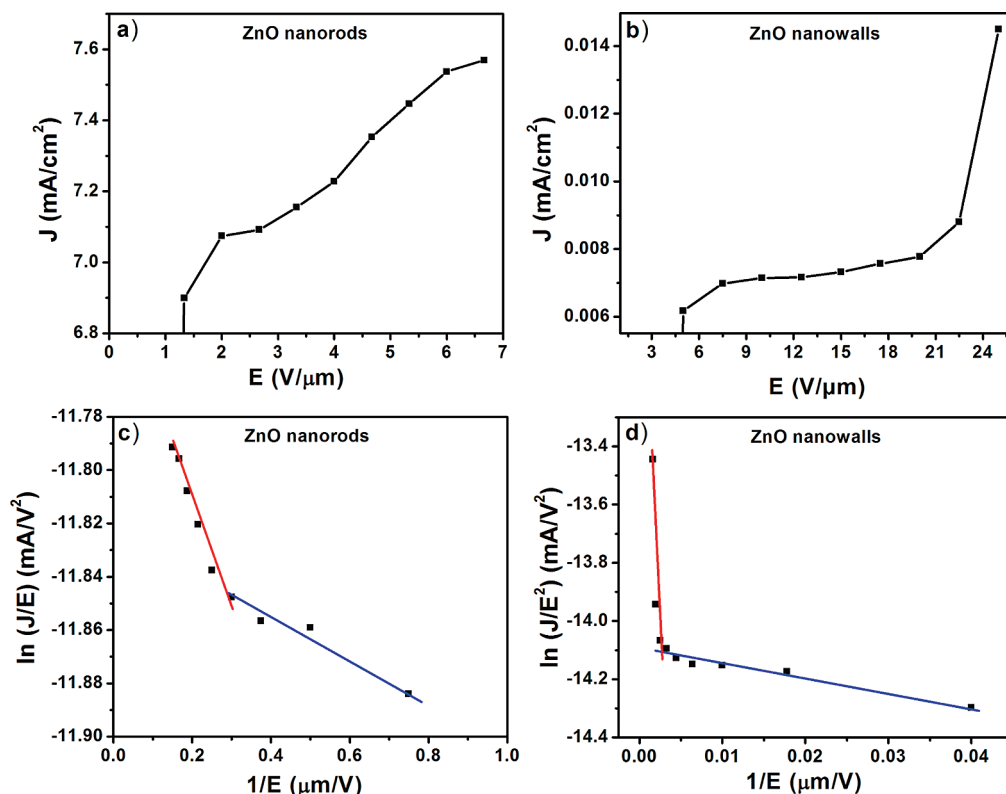
FIGURE 6. Field-emission curves: (a, b) $J-E$ plots of ZnO nanorods and nanowalls and (c, d) Fowler−Nordheim (F−N) plots of ZnO nanorods and nanowalls.

Si substrate, though there was large lattice mismatch between ZnO and Si and formation of native oxide layer on Si substrate.

3.3. Field Emission Studies. The unique vertically aligned ZnO nanowalls and nanorods are suitable for applications of field emission devices (29). Field emission characteristics of the ZnO nanowalls and nanorods grown on GaN and Si substrates, respectively, were investigated. The field emission study was performed at a base pressure of 1.5×10^{-5} Torr. Figure 6a shows the field emission curve of the current density as a function of electric field ($J-E$) for the ZnO nanowalls and nanorods, with cathode-to-anode spacing of 40 and 150 μm, respectively. The turn-on field of the ZnO nanorods and nanowalls were 2 V/μm (at 7.1 mA/cm^2) and 12.5 V/μm (at 7 μA/cm^2), respectively. The threshold field of the ZnO nanorods and nanowalls were 6.7 V/μm (at 7.5 mA/cm^2) and 25 V/μm (14 μA/cm^2), respectively. A low turn-on field of 2 V/μm was achieved for ZnO nanorods compared with ZnO nanospikes (30), nanorods (31), and nanoneedles (32). This turn-on field value is comparable with the values of ZnO nanopins (33) and microtowers (34). The turn-on field of ZnO nanorods is lower than the nanowalls. In addition to that, the current density (J) of the ZnO nanorods (7.7 mA/cm^2) is higher compared to those of the ZnO nanowalls (in the present work) and the previous reports. Pradhan et al. (30) achieved a J of 1.3 mA/cm^2 at 7 V/μm for ZnO nanospikes which is six times smaller than the J of the ZnO nanorods.

Figure 6b shows the Fowler−Nordheim (F−N) plot of the $J-E$ curves, i.e., ln(J/E^2) ∼ 1/E, for ZnO nanowalls and

nanorods. The F−N plot of ZnO nanostructures shows the two-slope behavior, as reported earlier (35). The nonlinearity in the F−N plot is the typical characteristic of the semiconductor material. The mechanism of the multistage slope phenomena is not clear yet. It has been explained on the basis of the energy band, adsorbents, and defects (35). The F−N plots have two slopes in this study and correlate well with the reports by Yuvaraj et al. (36) and Ramgir et al. (37). Ramgir et al. (37) reported smaller and larger β values in the higher and lower field regions, respectively. The two-slope behavior was explained on the basis of the electron emission from the conduction band (CB) and valence bands (VB). The electron emission occurs from the CB ($\Phi = 5.3$ eV) in the lower field. When the applied field is increased further, the electrons in the VB, i.e., 3.37 eV below the CB, contribute to the emission current together with the electrons from the CB. Now, the effective work function is $\Phi_0 = \Phi + E_g = 5.3 + 3.37 = 8.67$ eV. In this study, different slope values were observed in the lower and higher field, similar to Ramgir et al. (37). According to the F−N theory, the slope of the F−N plot is equal to $-6830 \Phi^{3/2}/\beta$, where Φ is the work function and β is the field enhancement factor (36). The β value for the ZnO nanowalls and nanorods were calculated using $\Phi = 5.3$ eV in the lower field and $\Phi_0 = 8.67$ eV in the higher field. The β-factor values have been listed in Table 1. The estimated β-factor of the ZnO nanorods is higher than that of the ZnO nanowalls, which is also consistent with the lower turn-on field of the nanorods. The experiment was repeated five times to check the consistency of the results. The same

ACS **APPLIED** MATERIALS & INTERFACES

Table 1. Calculated β-Factor Values of ZnO Nanorods and Nanowalls

	field enhancement factor (β)	
	lower field ($\Phi = 5.3$ eV)	higher field ($\Phi_0 = 8.67$ eV)
ZnO nanorods	10×10^5	4×10^5
ZnO nanowalls	16 862	515

FIGURE 8. Schematic cross sectional view of (a) ZnO nanorods and (b) ZnO nanowalls.

trend was observed in all experiments. Figure 7 shows the error limit (2 %) of $J-E$ and F−N plots of ZnO nanorods and nanowalls.

The FE performance of the nanostructures can be improved mainly by three factors. (1) Morphology of nanostructures such as the "tiplike" feature to increase the field enhancement factor. (2) Aligned nanostructures to enhance the emission current density and to increase the emission efficiency. (3) Doping can reduce the electron tunneling barrier. On the other hand, the screening effect and high resistivity are the detrimental factors for the FE performance of nanostructures (38, 39). The higher the field enhancement factor (β), the better is the emission. The intrinsic β-factor is related to the aspect ratio (h/r) for nanorods, where h is the height and r is the radius (30). The diameter of the ZnO nanorods varies from top to the bottom. The tapered tips at the end of ZnO nanorods is obvious from the cross sectional view of Figure 1f. The average diameter and length of ZnO nanorods are ∼300 ± 50 nm and ∼3 ± 0.1 μm, respectively. The aspect ratio of ZnO nanorod is 10. The diameter of the ZnO nanorod tip is ∼60 ± 5 nm. The aspect ratio of the ZnO nanorod tip is 50. Similarly, the aspect ratio of the nanowalls

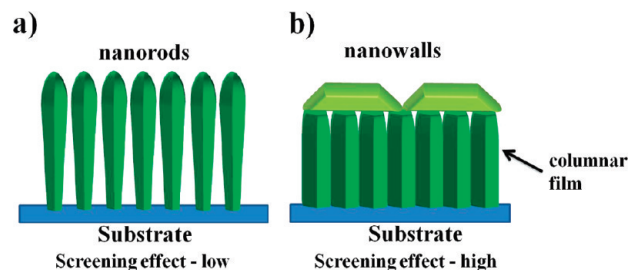can be measured using h/w, where w is the width. The width and height of the ZnO nanowalls were ∼120 ± 50 nm and ∼1.2 ± 0.1 μm, respectively. The aspect ratio of the nanowalls is 10. The width of the ZnO nanowalls decreases from top to the bottom. The width of the nanowalls ledge is ∼35 ± 5 nm. The aspect ratio is 34. The growth of dense ZnO columnar film followed by growth of interlinked nanowalls can be clearly seen in Figures 1d and 8b. The high density of the nanostructures reduces the emission current because of the screening effect, which prevents the field from concentrating on the edge of the emitters (38). In this study, the nanowalls with underlying dense columnar thin film can have high screening effect whereas vertically aligned and separated nanorods (Figures 1f and 8a) have relatively low screening effect. Hence, the high β-factor of ZnO nanorods can be attributed to the high aspect ratio of the tip with low screening effect, which in turn increase the effective field at
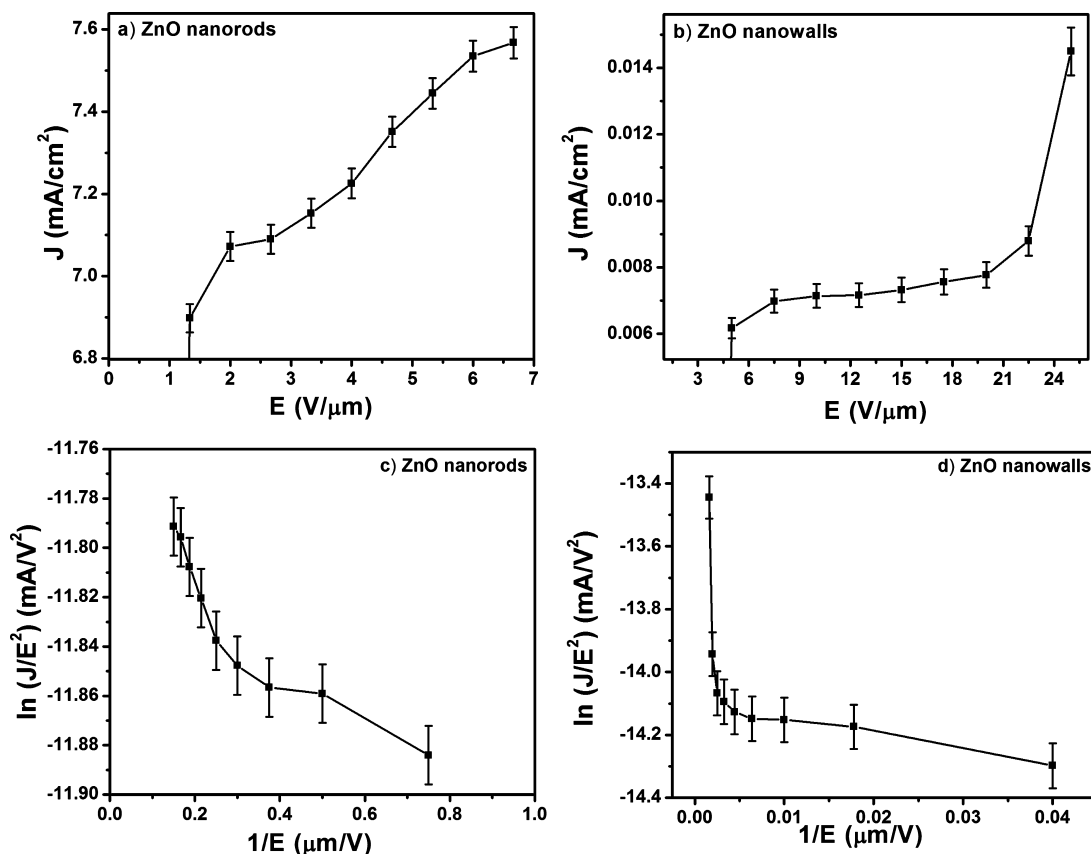

FIGURE 7. $J-E$ and F−N error limit plot of (a,c) ZnO nanorods and (b,d) nanowalls.

the end of the nanorods tip (6). Pradhan et al. reported a higher β-factor in nanopillars than in the nanowalls (40).

In addition to the tiplike feature and low screening effect, nanorods are vertically aligned on the substrate and have good crystallinity. Pradhan et al. (30) reported 2 orders of high current density in nanospikes, which had a tiplike feature and good crystallinity, compared to the nanopillars. Similarly, in this study, high current density was obtained for ZnO nanorods compared to the nanowalls. On the other hand, the alignment/orientation of nanorods is also very important for the field emission performance. From Figure 1f, it is clear that the ZnO nanorods on the cathode are pointing toward the anode, implying that all nanorods can contribute to the field emission. Hence, the low turn-on field, high current density, and large β value of ZnO nanorods can be attributed to the high aspect ratio of the tapered nanorod tip, low screening effect, and good vertical alignment compared with ZnO nanowalls.

4. CONCLUSIONS

The influence of the substrates on the morphology of ZnO nanostructures was studied using high-pressure PLD. The FE-SEM micrographs clearly show the growth of vertically aligned ZnO nanorods on Al_2O_3 and Si substrates whereas ZnO nanowalls were observed on GaN substrates. The small lattice mismatch between ZnO and GaN substrate led to the growth of dense columnar film followed by the formation of nanowalls. An intense E_{2H} Raman mode and strong NBE emission with negligible oxygen vacancy (V_O) confirmed that the ZnO nanorods grown on Si have better crystalline and optical properties compared with the ZnO nanostructures grown on GaN and Al_2O_3 substrates. The good field emission properties including a low turn-on field of 2 V/μm, a high current density of 7.7 mA/cm^2, and a large β-factor were achieved on the ZnO nanorod emitters. These ZnO nanorods emitters can effectively be used as cathodes in the applications of field emission devices.

REFERENCES AND NOTES

(1) Lin, Y. F.; Jian, W. B. *Nano Lett.* **2008**, *8*, 3146.
(2) Wang, X.; Summers, C. J.; Wang, Z. L. *Nano Lett.* **2004**, *4*, 423.
(3) Wang, X.; Song, J.; Wang, Z. L. *J. Mater. Chem.* **2007**, *17*, 711.
(4) Wan, Q.; Li, Q. H.; Chen, Y. J.; Wang, T. H.; He, X. L.; Li, J. P.; Lin, C. L. *Appl. Phys. Lett.* **2004**, *84*, 3654.
(5) Minami, T. *Semicond. Sci. Technol.* **2005**, *20*, S35.
(6) Yang, Y. H.; Wang, B.; Xu, N. S.; Yang, G. W. *Appl. Phys. Lett.* **2006**, *89*, 043108.
(7) Okada, T.; Kawashima, K.; Nakata, Y.; Ning, X. *Jpn. J. Appl. Phys.* **2005**, *44*, 688.
(8) Premkumar, T.; Manoravi, P.; Panigrahi, B. K.; Baskar, K. *Appl. Surf. Sci.* **2009**, *255*, 6819.
(9) Hong, Y. J.; Jung, H. S.; Yoo, J.; Kim, Y. J.; Lee, C. H.; Kim, M.; Yi, G. C. *Adv. Mater.* **2009**, *21*, 222.
(10) Huang, M. H.; Wu, Y.; Feick, H.; Tran, N.; Weber, E.; Yang, P. *Adv. Mater.* **2001**, *13*, 113.
(11) Kong, X. Y.; Wang, Z. L. *Appl. Phys. Lett.* **2004**, *84*, 975.
(12) Lu, J. G.; Ye, Z. Z.; Huang, J. Y.; Zhu, L. P.; Zhao, B. H.; Wang, Z. L.; Fujita, S. *Appl. Phys. Lett.* **2006**, *88*, 063110.
(13) Ng, H. T.; Li, J.; Smith, M. K.; Nguyen, P.; Cassel, A.; Han, J.; Meyyappan, M. *Science* **2003**, *300*, 1249.
(14) Kim, S. W.; Park, H. K.; Yi, M. S.; Park, N. M.; Park, J. H.; Kim, S. H.; Maeng, S. L.; Choi, C. J.; Moon, S. E. *Appl. Phys. Lett.* **2007**, *90*, 033107.
(15) Wu, C. C.; Wu, D. C.; Lin, P. R.; Chen, T. N.; Horng, R. H. *Nanoscale Res. Lett.* **2009**, *4*, 344.
(16) Cao, B. Q.; Matsumoto, T.; Matsumoto, M.; Higashihata, M.; Nakamura, D.; Okada, T. *J. Phys. Chem. C* **2009**, *113*, 10975.
(17) Verma, H.; Mukherjee, D.; Witanachchi, S.; Mukherjee, P.; Batzill, M. *J. Cryst. Growth* **2010**, *312*, 2012.
(18) Özgür, Ü.; Alivov, Ya. I.; Liu, C.; Teke, A.; Reshchikov, M. A.; Doğan, S.; Avrutin, V. *J. Appl. Phys.* **2005**, *98*, 041301.
(19) Hartanto, A. B.; Ning, X.; Nakata, Y.; Okada, T. *Appl. Phys. A: Mater. Sci. Process.* **2004**, *79*, 299.
(20) Li, W. J.; Shi, E. W.; Zhong, W. Z.; Yin, Z. W. *J. Cryst. Growth* **1999**, *203*, 186.
(21) Jeong, J. S.; Lee, J. Y.; Cho, J. H.; Lee, C. J.; An, S. J.; Yi, G. C.; Gronsky, R. *Nanotechnology* **2005**, *16*, 2455.
(22) Laudise, R. A.; Ballman, A. A. *J. Phys. Chem.* **1960**, *64*, 688.
(23) Wang, X.; Song, J.; Li, P.; Ryou, J. H.; Dupuis, R. D.; Summers, C. J.; Wang, Z. L. *J. Am. Chem. Soc.* **2005**, *127*, 7920.
(24) Singamaneni, S.; Gupta, M.; Yang, R.; Tomczak, M. M.; Naik, R. R.; Wang, Z. L.; Tsukruk, V. V. *Nano* **2009**, *3*, 2593.
(25) Zhu, X.; Wu, H.; Yuan, Z.; Kong, J.; Shen, W. *J. Raman Spectrosc.* **2009**, *40*, 2155.
(26) Sahoo, S.; Arora, A. K.; Sridharan, V. *J. Phys. Chem. C* **2009**, *113*, 16927.
(27) Lin, B.; Fu, Z.; Jia, Y. *Appl. Phys. Lett.* **2001**, *79*, 943.
(28) Jeong, S. H.; Kim, B. S.; Lee, B. T. *Appl. Phys. Lett.* **2003**, *82*, 2625.
(29) Lee, C. J.; Lee, T. J.; Lyu, S. C.; Zhang, Y.; Ruh, H.; Lee, H. J. *Appl. Phys. Lett.* **2002**, *81*, 3648.
(30) Pradhan, D.; Kumar, M.; Ando, Y.; Leung, K. T. *Appl. Mater. Interfaces* **2009**, *1*, 789.
(31) Yang, C. J.; Wang, S. M.; Liang, S. W.; Chang, Y. H.; Chen, C.; Shieh, J. M. *Appl. Phys. Lett.* **2007**, *90*, 033104.
(32) Zhang, Z.; Yuan, H.; Zhou, J.; Liu, D.; Luo, S.; Miao, Y.; Gao, Y.; Wang, J.; Liu, L.; Song, L.; Xiang, Y.; Zhao, X.; Zhou, W.; Xie, S. *J. Phys. Chem. B* **2006**, *110*, 8566.
(33) Xu, C. X.; Sun, X. W. *Appl. Phys. Lett.* **2003**, *83*, 3806.
(34) Xu, F.; Yu, K.; Li, Q.; Zhu, Z.; Yao, T. *J. Phys. Chem. C* **2007**, *111*, 4099.
(35) Xu, C. X.; Sun, X. W.; Fang, S. N.; Yang, X. H.; Yu, M. B.; Zhu, G. P.; Cui, Y. P. *Appl. Phys. Lett.* **2006**, *88*, 161921.
(36) Yuvaraj, D.; Kaushik, R.; Narashimarao, K. *Appl. Mater. Interfaces* **2010**, *2*, 1019.
(37) Ramgir, N. S.; Late, D. J.; Bhise, A. B.; Mulla, I. S.; More, M. A.; Joag, D. S.; Pillai, V. K. *Nanotechnology* **2006**, *17*, 2730.
(38) Wang, X. D.; Zhou, J.; Lao, C. S.; Song, J. H.; Xu, N. S.; Wang, Z. L. *Adv. Mater.* **2007**, *19*, 1627–1631.
(39) She, J.; Xiao, Z.; Yang, Y.; Deng, S.; Chen, J.; Yang, G.; Xu, N. *ACS Nano* **2008**, *2*, 2015.
(40) Pradhan, D.; Kumar, M.; Ando, Y.; Leung, K. T. *J. Phys. Chem. C* **2008**, *112*, 7093.

AM100539Q